13474–13487 *Nucleic Acids Research, 2014, Vol. 42, No. 22* *Published online 20 November 2014*
doi: 10.1093/nar/gku1157

The phosphate clamp: sequence selective nucleic acid binding profiles and conformational induction of endonuclease inhibition by cationic Triplatin complexes

Andreea Prisecaru[1], Zara Molphy[1], Ralph G. Kipping[2], Erica J. Peterson[2], Yun Qu[2], Andrew Kellett[1,*] and Nicholas P. Farrell[2]

[1]School of Chemical Sciences and National Institute for Cellular Biotechnology, Dublin City University, Glasnevin, Dublin 9, Ireland and [2]Department of Chemistry, Virginia Commonwealth University, Richmond, VA 23284-2006, USA

Received September 19, 2014; Revised October 28, 2014; Accepted October 29, 2014

ABSTRACT

The substitution-inert polynuclear platinum(II) complex (PPC) series, [{*trans*-Pt(NH$_3$)$_2$(NH$_2$(CH$_2$)$_n$NH$_3$)}$_2$-μ-(*trans*-Pt(NH$_3$)$_2$(NH$_2$(CH$_2$)$_n$NH$_2$)$_2$}](NO$_3$)$_8$, where *n* = 5 (AH78P), 6 (AH78 TriplatinNC) and 7 (AH78H), are potent non-covalent DNA binding agents where nucleic acid recognition is achieved through use of the 'phosphate clamp' where the square-planar tetra-am(m)ine Pt(II) coordination units all form bidentate N–O–N complexes through hydrogen bonding with phosphate oxygens. The modular nature of PPC–DNA interactions results in high affinity for calf thymus DNA (K_{app} ~5 x 10^7 M^{-1}). The phosphate clamp–DNA interactions result in condensation of superhelical and B-DNA, displacement of intercalated ethidium bromide and facilitate cooperative binding of Hoechst 33258 at the minor groove. The effect of linker chain length on DNA conformational changes was examined and the pentane-bridged complex, AH78P, was optimal for condensing DNA with results in the nanomolar region. Analysis of binding affinity and conformational changes for sequence-specific oligonucleotides by ITC, dialysis, ICP-MS, CD and 2D-^{1}H NMR experiments indicate that two limiting modes of phosphate clamp binding can be distinguished through their conformational changes and strongly suggest that DNA condensation is driven by minor-groove spanning. Triplatin-DNA binding prevents endonuclease activity by type II restriction enzymes BamHI, EcoRI and SalI, and inhibition was confirmed through the development of an on-chip microfluidic protocol.

INTRODUCTION

The X-ray crystal structure of the Dickerson–Drew dodecamer (DDD, [d(CGCGAATTCGCG)]$_2$) with the non-covalently binding trinuclear platinum compound TriplatinNC (AH78), Scheme 1, described a new mode of ligand–DNA recognition distinct from the conventional modes of intercalation and groove binding (NDB entry 2DYW) (1). Hydrogen bonding with phosphate oxygens results in either backbone tracking or groove spanning through formation of 'phosphate clamps' where the square-planar tetra-am(m)ine Pt(II) coordination units all form bidentate N–O–N complexes with phosphate oxygen OP atoms, Figure 1. The generality of the motif has been confirmed by a second crystal and molecular structure with TriplatinNC-A (AH44)—that is with $L = NH_3$ (6+) instead of –NH$_2$(CH$_2$)$_6$NH$_3^+$ (8+); see Scheme 1 (2). In both cases, the conformation in the DDD–Phosphate Clamp complexes differs significantly from that of the native structure (NDB entry BDL084). The structural distortions caused are principally axial bending and axial path length shortening ratio, which are significantly greater than those of the control DDD. Helical parameters are perturbed and the minor-groove width profile is modestly impacted. The axial bending is similar to that induced by the cisplatin intrastrand 1,2-GG adduct, (3), but achieved solely through H-bonding and electrostatic interactions. The phosphate clamp is analogous to that of the guanidino group of arginine which shows an analogous, but attenuated clamping ability in which two OP atoms form a clamp-like structure, the Arginine Fork (4,5).

The discovery of new molecular mechanisms by which small molecules modify DNA structure, reactivity and biological repair contributes significantly to potential drug development as DNA is a clinically important target (6,7). The broad class of polynuclear platinum complexes (PPCs)

*To whom correspondence should be addressed. Tel: +353 1 700 5461; Fax: +353 1 7005484; Email: andrew.kellett@dcu.ie
Correspondence may also be addressed to Nicholas P. Farrell. Tel: +1 804 8286320; Fax: +1 804 828 8599; Email: npfarrell@vcu.edu

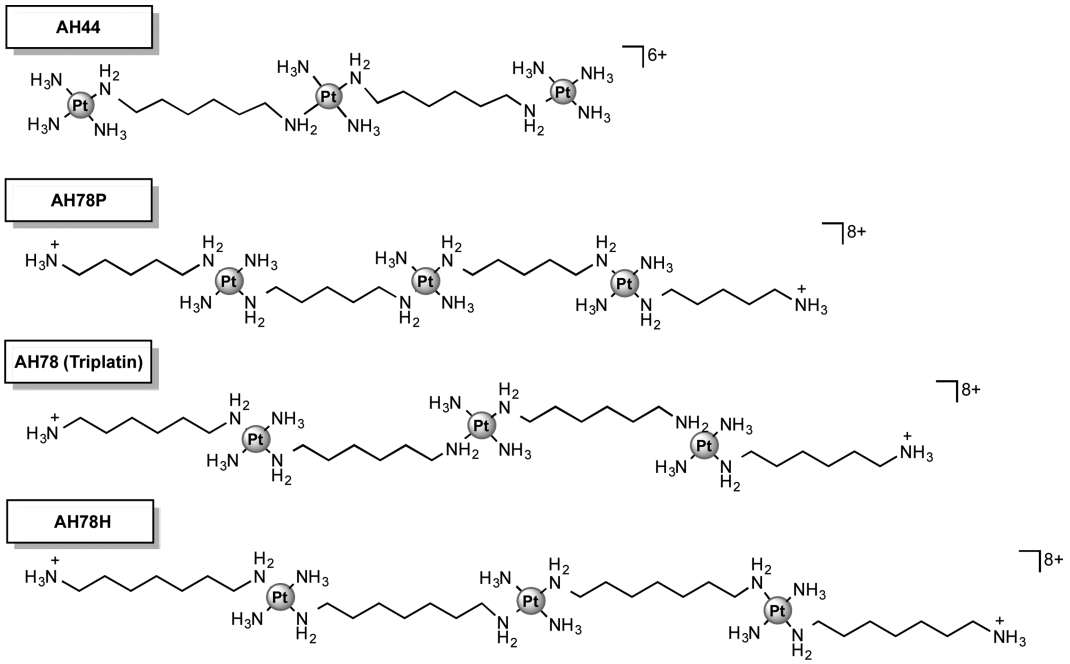

Scheme 1. Molecular structures of $[\{Pt(NH_3)_3\}_2\text{-}\mu\text{-}\{trans\text{-}Pt(NH_3)_2(NH_2(CH_2)_6NH_2)_2\}]^{6+}$ (AH44, TriplatinNC-A) and $[\{trans\text{-}Pt(NH_3)_2(NH_2(CH_2)_nNH_3)\}_2\text{-}\mu\text{-}(trans\text{-}Pt(NH_3)_2(NH_2(CH_2)_nNH_2)_2\}]^{8+}$ cations where $n = 5$ (AH78P), 6 (AH78H, TriplatinNC) and 7 (AH78H).

may now be divided into those complexes capable of Pt-DNA covalent bond formation such as BBR3464, the only 'non-classical' platinum drug to enter human clinical trials, and those 'non-covalently binding' compounds depicted in Scheme 1 with inherently substitutionally inert PtN_4 coordination spheres (8). Specifically, TriplatinNC has demonstrated interesting biological activity in its own right. The complex is cytotoxic at micromolar concentrations, similar to cisplatin, in a range of human tumor cell lines but is unaffected by serum degradation (9). The induction of apoptosis in tumor cells suggests that covalent Pt-DNA bond formation is not a prerequisite for antitumor activity for compounds with high DNA affinity, a further shift in the structure–activity paradigm of platinum antitumor agents. Simultaneous multi-element imaging using NanoSIMS (nano-scale secondary ion mass spectrometry), exploiting the novel combination of ^{195}Pt and ^{15}N in platinum-am(m)ine antitumor drugs, confirmed localization of TriplatinNC in the nucleolus of MCF7 cells (10), with implications for interaction with ribosomal DNA and/or RNA within the nucleolus.

The nature of the PPC chemotype means that it is a discrete and modular DNA binding device with high potential as a drug-design scaffold. Within the non-covalently binding motif, possible systematic changes include dinuclear complexes such as $[\{Pt(NH_3)_3\}_2\text{-}\mu\text{-spermidine}]^{5+}$ and $[\{Pt(NH_3)_3\}_2\text{-}\mu\text{-spermine}]^{6+}$ connected via polyamine central linkers rather than the {Pt(tetraamine)} trinuclear unit, and the use of the 'dangling' amine versus NH_3 as ligand to add further overall charge diversity (8). Binding studies of AH44 to DNA polymers of varying base composition—or topology—revealed high affinity and limited discrimination in terms of binding constant and mode (11,12). Both TriplatinNC and AH44 are significantly more effective nucleic acid condensing agents compared to spermine (11,12). A further modification to affect DNA binding interactions is variation of alkanediamine chain length in the trinuclear structures of Scheme 1. In principle, modifying distances between phosphate clamp coordination units (12.46 Å from NDB entry 2DYW) could be used to maximize overlap with phosphate–phosphate distances of RNA and differing DNA conformations. In this contribution we describe the effects of TriplatinNC congeners, Scheme 1, on DNA binding affinity and inhibition of endonuclease enzyme recognition by various biophysical and molecular biological methods. Preliminary comparisons with tRNA affinity are made and in all cases the minor-groove binding agents, netropsin and pentamidine, along with the cationic cobalt(III) complex, $[Co(NH_3)_6]^{3+}$, were examined to delineate new properties within this class of drug molecule. A general question in all of this work is: how do the solution binding properties reflect the crystallographically determined modes of groove spanning and backbone tracking as shown in Figure 1? This contribution demonstrates that the two distinctive limiting interaction modes may be distinguished by their formational dependence on tertiary DNA helical topology and G·C content and suggests that DNA condensation is driven by minor-groove recognition.

MATERIALS AND METHODS

Chemicals and deoxyribonucleic acid sodium salt from salmon testes were purchased from Sigma Aldrich (Ireland) and used without further purification. Ultra Pure calf-thymus DNA (CT-DNA, Cat.15633-019) and transfer RNA (tRNA, AM7119) was supplied from Invitrogen, supercoiled plasmid DNA (pUC19, Cat. N3041L) and restriction endonucleases AatII (R0117 S; 20 000 U/ml), BamHI

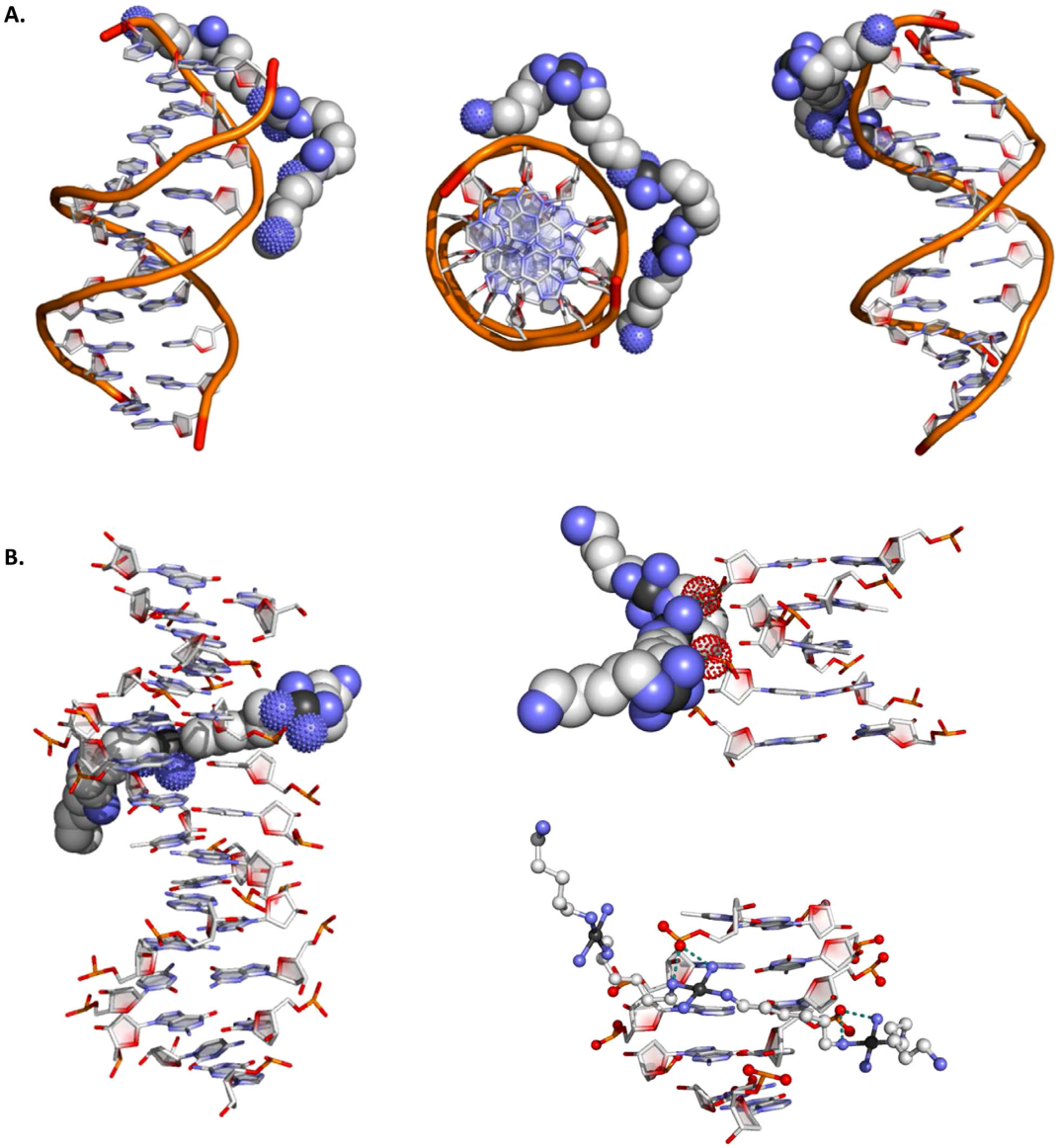

Figure 1. Perspective views of the double-stranded B-DNA Dickerson–Drew dodecamer bound to TriplatinNC via backbone tracking (**A**) and groove-spanning (**B**) modes (1, NDB entry 2DYW). DNA backbone (connecting P positions), orange; carbon, gray80; oxygen, red; nitrogen, slate (all in cartoon mode). Triplatin complex (space-filling mode) atoms colored as DNA; platinum, gray30. Platinum(II) amine nitrogen atoms, and selected phosphate coordinated oxygen atoms, engaged in phosphate clamping shown with dotted surface. Figures generated by PyMOL Molecular Graphics System, Version 1.5.0.4 Schrödinger, LLC.

(R0136 S; 20 000 U/ml), EcoRI (R0101 S; 20 000 U/ml) and SalI (R 0138 S; 20 000 U/ml) were supplied by NEB. Fluorescence measurements were conducted using a Bio-Tek Synergy HT multi-mode microplate reader; viscosity was measured with DV-II Programmable Digital Viscometer equipped with Enhanced Brookfield UL Adapter; thermal melting analysis was carried out on an Agilent Cary 100 dual beam spectrophotometer equipped with a 6 × 6 Peltier system and microfluidic chip experiments were conducted on the Bioanalyzer 2100 platform using DNA 7500 chips supplied by Agilent Technologies Ireland.

Preparation of triplatin complexes [{*trans*-$Pt(NH_3)_2(NH_2(CH_2)_nNH_3)\}_2$-μ-*trans*-$Pt(NH_3)_2(NH_2(CH_2)_nNH_2)_2]$ $(NO_3)_8$

The 'non-covalent' compounds with varying chain lengths (n = 5,6,7) were synthesized by adapting published procedures (8,13). The complexes AH78P, AH78 (TriplatinNC) and AH78H were characterized by C,H,N, elemental analysis and ^{1}H and ^{195}Pt nuclear magnetic resonance (NMR) spectroscopy. Purity was confirmed by High Performance Liquid Chromatography (HPLC). For n = 5, ^{1}H NMR (δ(^{1}H), D_2O, ppm): 2.99 (t, 4H); 2.66 (t,12H); 1.66 (m, 16H); 1.38 (m,8H). δ (^{195}Pt NMR, D_2O, ppm): −2675. HPLC Purity 99.8%. For n = 6, ^{1}H NMR (δ(^{1}H), D_2O, ppm): 2.95

(t, 4H); 2.62 (t,12H); 1.60 (m, 16H); 1.38 (m,16H). δ (^{195}Pt NMR, D_2O, ppm): −2680. HPLC Purity 99.0%. For n = 7, ^{1}H NMR (δ(^{1}H), D_2O, ppm): 2.98 (t, 4H); 2.62 (t,12H); 1.62 (m, 16H); 1.32 (m,24H). δ (^{195}Pt NMR, D_2O, ppm): −2680. HPLC Purity 99.0%.

DNA binding experiments

Competitive ethidium bromide displacement. Experiments were conducted in a similar manner to the high-throughput method reported by Kellett *et al.* (14). Each drug concentration was measured in triplicate, on at least two separate occasions, and the apparent binding constants were calculated using $K_{app} = K_b$ x $12.6/C_{50}$ where $K_b = 8.80 \times 10^6$ M(bp)$^{-1}$ (S1) (K_{app} = apparent binding constant).

DNA binding kinetic studies. A working solution of 20.0 μM of calf thymus DNA (ctDNA) along with 25.2 μM of ethidium bromide (EtBr) in HEPES buffer (80 mM, pH = 7.2) and NaCl (40 mM) was prepared. 50 μl of DNA-EtBr working solution were placed in each well of a 96-well microplate with the exception of the controls, which contained 100 μl of buffer. A 1.0 μM aliquot of test complex was then added to each well plate such that an r value of 0.1 was achieved (r = [complex]/[ctDNA], ϵ_{max} = 12824 M(bp)$^{-1}$ cm^{-1} for ctDNA) and the volume was adjusted to 100 μl such that the final concentration of CT-DNA and EtBr was 10.0 μM and 12.6 μM, respectively. Fluorescence measurements were recorded using a Bio-Tek synergy HT multi-mode microplate reader with excitation and emission wavelengths being set to 530 and 590 nm. Kinetic studies were analyzed over a 1-h period at room temperature with measurements taken at 68-s intervals.

DNA fluorescence quenching. Experiments were conducted in a similar manner to the high-throughput method reported previously (14).

Viscosity studies (15). A 15-ml solution containing 1×10^{-3} M deoxyribonucleic acid sodium salt from double-stranded salmon testes (salmon testes DNA (stDNA), D1626-1G—Sigma-Aldrich) was prepared in 80-mM HEPES buffer for each working experiment. Stock solutions prepared in nuclease-free H_2O were added according to the gradual increasing [compound/DNA] ratios of 0.02, 0.04, 0.06, 0.08, 0.10, 0.12, 0.14, 0.16, 0.18 and 0.2. Viscosity values, η, (unit: cP) were directly obtained by running 0# spindle in working samples at 60 rpm via DV-II-Programmable Digital Viscometer equipped with Enhanced Brookfield UL Adapter at room temperature. Data were presented as η/η_o versus [compound]/[DNA] ratio, in which η_o and η refer to viscosity of each DNA working sample in the absence and presence of complex.

ctDNA thermal melting analysis (16). In a final volume of 1 ml using black-walled quartz cuvettes (Starna) with tight-fitting seals, 50-mM potassium phosphate buffer (pH = 7.8), 2.0-mM NaCl and CT-DNA were added to give a final absorbance of 0.5 absorbance units at 260 nm. Stock solutions of platinum complexes prepared in nuclease-free H_2O, minor-groove binders (netropsin and pentamidine), the cobalt(III) complex $[Co(NH_3)_6](NO_3)_3$, and the intercalator EtBr were prepared in 80 mM HEPES. A 3.75-μM aliquot of test reagent was then added to each cuvette such that an r value of 0.05 was achieved (r = [compound]/[ctDNA], ϵ_{max} = 6600). Thermal melting measurements were recorded at 260 nm at 0.5-s intervals over a temperature range of 20–97°C. Temperature was calibrated for each measurement using a temperature probe placed in an identical black-walled cuvette containing 50 mM of phosphate buffer. The temperature was ramped at 3.5°C/min with data being collected every 0.5°C. The spectral bandwidth (SBW) was set to 1. Replicate samples were run in triplicate and the melting temperature, T_M (°C), was calculated using the built-in derivative method on the instrument.

Thermal melting analysis on modified DNA. The concentrations of nucleic acids (expressed as nucleotides) were determined spectrophotometrically using the extinction coefficients ϵ_{260} = 6000 M^{-1} cm^{-1} for ctDNA, ϵ_{260} = 6225 M^{-1} cm^{-1} for *Clostridium perfringens* (Type XII, Sigma) (17), ϵ_{262} = 6650 M^{-1}cm^{-1} for poly[d(A-T)$_2$] (16) and ϵ_{260} = 6000 M^{-1}cm^{-1} for poly(dA)-poly(dT) (18). The 100-μM polynucleotide DNA samples were incubated with TriplatinNC at a ratio r = 0.05 (r being the ratio of drug per nucleotide) in 10-mM $NaClO_4$ at 37°C for 1 h. All samples were degassed prior to measurement. The absorbance at 260 nm was recorded while the temperature was increased from 20 to 95°C at a rate of 0.5°C/min.

DNA association assay. 100-μM CT-DNA, poly(dA-dT)$_2$ or poly(dG-dC)$_2$ were incubated with 5-μM TriplatinNC (r = 0.05) at 37°C protected from light for 1 h in 10-mM phosphate buffer and 50-mM NaCl at pH 7.4. Subsequently the samples were divided into two equal parts. One mixture was used as control and the other one was dialyzed against the same buffer for 24 h. The buffer solution was exchanged every 8 h. The modified DNA was digested with 500-μl HNO_3 concentrated and 500-μl water at 95°C for 3 h. 1000 μl of water was added and the platinum content was determined by ICP-MS. The experiment was conducted thrice and the determined platinum concentrations were averaged.

Comparative binding of mithramycin toward poly(dG-dC)$_2$ in the presence and absence of TriplatinNC. Samples were prepared in buffer solutions containing 10-mM PO_4^{3-}, 50-mM NaCl and 10-mM $MgCl_2$ (pH 7.4). The concentrations of mithramycin A (ϵ_{400} = 10 000 M^{-1} cm^{-1}) and poly(dG-dC)$_2$ (ϵ_{254} = 8400 M^{-1} cm^{-1}) were determined spectrophotometrically. Poly(dG-dC)$_2$ was incubated with TriplatinNC at a ratio of 0.05 drug/nucleotide at 37°C for 1 h. Varying amounts of mithramycin A were added in the r range of 0.0–0.25 to modified and untreated DNA. The samples were kept for 24 h at 37°C in the dark. The final concentration of poly(dG-dC)$_2$ in the samples was 100 μM. Fluorescence spectra were recorded with a Cary Eclipse spectrofluorometer. To avoid photodegradation the fluorescence excitation wavelength was set to 470 nm. The absorbance of the samples at this wavelength was less than 0.05 with the inner filter effect therefore being neglected. Spectra were recorded in the range of 525–625 nm.

NMR analysis of TriplatinNC-modified DNA oligomers

NMR spectroscopy. The NMR spectra were recorded on a Bruker AVANCE III 600-MHz spectrometer (^{1}H, 600.1 MHz) fitted with a pulsed field gradient module and 5-mm inverse quadruple resonance (QXI) probe. The ^{1}H NMR chemical shifts are internally referenced to trimethylsilyl propionic acid (TSP). The two-dimensional [^{1}H,^{1}H] correlation spectroscopy (COSY) and nuclear Overhauser effect spectroscopy (NOESY) spectra were acquired with water suppression using the excitation sculpting, total correlation spectroscopy (TOCSY) spectra were recorded with the watergate 3-9-19 pulse sequence.

All samples were prepared in 99.99% D_2O or 8% D_2O/92% H_2O with 10-mM PO_4^{3-}, 300-mM NaCl and adjusted to pD 6 or pH 6 with DNO_3/NaOD or HNO_3/NaOH. All two-dimensional [^{1}H,^{1}H] NMR experiments were obtained with 1-mM oligomer and 1-mM oligomer with 1-mM TriplatinNC. The assignments of the resonances for the oligomers and in the presence of TriplatinNC were conducted in the standard manner as described in previous reports (19,20).

Endonuclease enzyme inhibition

Linearization of pUC19. Supercoiled plasmid pUC19 (2686 bp) was linearized by the AatI endonuclease according to the standard methods. Linear DNA was then purified from the enzymatic reaction using QIAquick PCR purification (QIAGEN) and quantified using the NanoDrop (ND-1000) spectrophotometer.

Inhibition study. In a typical binding experiment, 400 ng of linear pUC19 was mixed with a series of aliquots of platinum complexes prepared in nuclease-free H_2O (Ambion, AM9932) and the reaction mixture was incubated at 37°C for 24 h. Subsequent digestion experiments were performed by incubating the drug-treated and untreated primary digest of pUC19 with BamHI, EcoRI or SaII endonucleases. This reaction was carried out by adding 1 μl of restriction enzyme (20 000 U/ml), and 2.5-μl NEBuffer 3.1 (NEB) and/or 2.5-μl EcoRI buffer (where applicable) to the digestion reaction which was allowed to incubate at 37°C for 2.5 h. Reactions were then subjected to electrophoresis (in 1.0% agarose, stained as previously described). Reactions of BamHI and SalI were then examined using the DNA 7500 microfluidic chip prepared as per the manufacturers protocol with data being collected on the Agilent Bioanalyzer 2100 platform (http://www.genomics.agilent.com/en/Bioanalyzer-TapeStation-/?pgid = AG-PG-1).

Binding affinity of EtBr to ctDNA and tRNA

In a final volume of 1 ml, 100-μM EtBr, 20-mM NaCl and 50-mM potassium phosphate buffer (pH = 7.8) were added to quartz cuvettes (Starna) to give a final absorbance of ∼0.6 absorbance units at 480 nm (ϵ_{max} for EtBr). Titrations were then performed by adding aliquots of either ctDNA ($\epsilon_{260} = 12\,824\ M^{-1}\ cm^{-1}$) or tRNA ($\epsilon_{260} = 9250\ M^{-1}\ cm^{-1}$) to each cuvette and scans were performed every 5–10 min after thermal equilibrium had been reached at 25°C. The analysis was stopped when no change in the absorbance was observed upon addition of either ctDNA or tRNA. Hypochromicity and a bathochromic shift to 521 nm with isosbestic points at 509 nm for ctDNA was observed, and a shift to 518 nm with an isosbestic point at 512 nm for tRNA was observed in the binding analysis. Titrations were monitored at 25°C using an Agilent Cary 100 dual beam spectrophotometer equipped with a 6 × 6 multi-cell system. The intrinsic binding constants (K_b) for EtBr on ctDNA and tRNA were determined using the method outlined by Bard *et al.* (21) (Supplementary Figure S1).

tRNA binding

tRNA–ethidium fluorescence quenching. A working solution of 160.0-μM tRNA (Invitrogen AM7119, $\epsilon_{260} = 9250\ M^{-1}\ cm^{-1}$) expressed as molarity of the phosphate group for tRNA (22) along with 25.2-μM EtBr in HEPES buffer (80 mM, pH = 7.2) and NaCl (40 mM) was prepared. Stock solutions of metal complexes and metal salt were prepared in nuclease-free H_2O (Ambion, AM9932). 50 μl of the tRNA-EtBr working solution were placed in each well of a 96-well microplate with the exception of the blanks, which contained 100 μl of buffer. Serial aliquots of the tested compound were added to the working solutions and the volume was adjusted to 100 μl in each well such that the final concentration of tRNA and EtBr was 80.0 μM and 12.6 μM, respectively. The plate was allowed to incubate at room temperature for 1 h before analysis using a Bio-Tek synergy HT multi-mode microplate reader with excitation and emission wavelengths being set to 530 and 590 nm, respectively. Each drug concentration was measured in triplicate, and the apparent binding constants were calculated using $K_{app} = K_b \times 12.6/C_{50}$ where $K_b = 6.78 \times 10^4\ M(bp)^{-1}$ (K_{app} = apparent binding constant).

tRNA thermal melting analysis. In a final volume of 1 ml using Starna black-walled quartz cuvettes with tight-fitting seals, 50-mM potassium phosphate buffer (pH = 7.8), 1-M NaCl and tRNA were added to give a final absorbance of ∼1.1 absorbance units at 260 nm. Stock solutions of metal complexes were prepared in nuclease-free H_2O. An aliquot of test reagent was then added to each cuvette such that an r value of 0.1 was achieved (r = [compound]/[tRNA], $\epsilon_{max} = 9250\ M^{-1}cm^{-1}$ expressed as molarity of phosphate group for tRNA). Thermal melting measurements were recorded at 260 nm at 0.5-s intervals over a temperature range of 20–90°C. Temperature was calibrated for each measurement using a temperature probe placed in an identical black-walled cuvette containing 50 mM of phosphate buffer and 1-M NaCl. The temperature was ramped at 4°C/min with data being collected every 0.5°C. The SBW was set to 1. Replicate samples were run in triplicate and the overall melting temperature, T_M (°C), was calculated using the built-in derivative method on an Agilent Cary 100 dual beam spectrophotometer equipped with a 6 × 6 multi-cell system.

RESULTS AND DISCUSSION

Binding to calf thymus and stDNA

To identify DNA binding properties of this series, ctDNA and stDNA were examined through a variety of biophysi-

cal methods including EtBr fluorescent competition studies, fluorescence quenching of limited bound EtBr (23) and Hoechst dye 33258 (24), thermal melting and viscosity analysis. In all tests conducted, the minor-groove binding agents, netropsin and pentamidine, along with the cationic cobalt(III) complex, $[Co(NH_3)_6]^{3+}$, were examined as reference agents against which new properties of these phosphate clamping platinum(II) complexes could be identified.

Thermal melting on ctDNA (Table 1 and Supplementary Figure S2) revealed that netropsin extensively stabilized the thermal denaturation ($\Delta T_M = +7.47 \pm 0.50$) (25) while pentamidine and $[Co(NH_3)_6]^{3+}$ yielded either no, or negligible, effects under our tested conditions. Triplatin complexes all stabilized ctDNA melting temperature to a similar degree as netropsin (e.g. $\Delta T_M = +8.20 \pm 0.26$ for AH78) and by analogy it is likely that this effect arises through the groove spanning interaction where platinum(II) phosphate clamps form on opposing sides of the minor groove rather than backbone tracking along one single strand (1,2). Indeed, the minor groove, which is A·T-rich, is the first tract to melt within B-DNA (16) and thus groove-spanning Triplatin interactions at A·T sequences are likely to confer thermal stabilization on the nucleotide polymer.

Competitive fluorescence binding to EtBr-saturated ctDNA solutions was performed in triplicate using a high-throughput binding method (14) and results are shown in Supplementary Figure S3A and Table 1. The intrinsic binding constant (K_b) of EtBr was identified as 8.8×10^6 $M(bp)^{-1}$ through direct spectrophotometry (Supplementary Figure S1) and the apparent DNA binding constants (K_{app}) for the tested compounds were calculated based on the K_b of EtBr and concentration required to displace 50% of this bound fluorophore. The K_{app} values for netropsin and pentamidine were identified as 2.55×10^6 and 8.77×10^5 $M(bp)^{-1}$, respectively, while the cobalt(III) complex and metal free diamine ligand, 1,6-hexanediamine, were unable to displace 50% of bound intercalator up to 300 μM. Triplatin complexes were highly efficient at displacing bound EtBr with all three having almost identical binding constants of $\sim 5 \times 10^7$ $M(bp)^{-1}$. In order to identify their relative binding kinetics to DNA, each complex was examined under constant fluorescence measurement at 10% drug load (r = [complex]/[DNA] = 0.10), in the presence of saturated EtBr bound ctDNA (Supplementary Figure S3C). Hexane- and heptanediamine-bridged complexes (AH78 and AH78H) were 50% bound by ∼34 min while for the pentanediamine complex a considerably faster interaction was evident at ∼4.5 min.

In order to characterize condensation of DNA, viscosity experiments were conducted using stDNA fibers exposed to the Triplatin series at drug:DNA ratios (r) between 0.01 and 0.20 (Supplementary Figure S3B and Table 1). As expected, EtBr exhibited classical intercalative binding with concentration-dependent relative viscosity enhancement (26) while the groove-binding agent, netropsin, had negligible influence only. The cobalt(III) cation, $[Co(NH_3)_6]^{3+}$, condensed DNA, in broad agreement with previous work by Kankia *et al.* (27). Triplatin complexes compact and precipitate DNA and this effect is pronounced with distinctive η/η_o values for all three complexes. Indeed, viscosity by Triplatin molecules decreases in linear fashion with the overall trend almost dwarfing the relative viscosity changes of the standard tested agents. To mitigate the effects of long-range coiling, which can significantly impact viscosity (28), high molecular weight stDNA fibers were vigorously sheared (see Supplementary S4) (29) before being examined under identical conditions described above. Long-range coiling effects of non-sheared stDNA can be discounted as Triplatin had greater condensation effects on sheared stDNA (Supplementary Figure S5). We postulate that shorter DNA fragments aggregate more efficiently due to enhanced intramolecular phosphate clamping interactions driven by greater accessibility to smaller nucleotide fragments.

Binding mode interactions were determined using fluorescence quenching of limited bound EtBr and Hoechst 33258 to ctDNA (Figure 2). The minor-groove binding agents, netropsin and pentamidine, and the cationic cobalt(III) complex—which has surface binding properties on nucleic acids (30)—displaced the minor-groove fluorogen Hoechst 33258 with greater specificity than intercalated EtBr. In contrast to these standards, the Triplatin series exhibited unique profiles. Firstly, the Triplatin series efficiently ablated EtBr fluorescence with quenching values (Q) of the order of ∼5 μM. Secondly, the complexes induce cooperative binding of Hoechst 33258 at the minor groove as evident through fluorescence enhancement by ∼25% within each assay. The cooperative binding of Hoechst 33258 can be understood from the minor-groove width opening caused by the phosphate clamps as structurally characterized in the Dickerson–Drew dodecamer (1,2,31). This interaction may conceivably facilitate selective binding by A·T targeting molecules such as Hoechst dye. The quenching of EtBr fluorescence, in contrast, may be connected to a conformational change, or condensation effect, on the tertiary structure of DNA that disfavors intercalative penetration.

Base-specific nucleic acid interactions

The 'classical' minor-groove binders such as netropsin and Hoechst 32258 by definition show distinct binding preferences for A-T tracts. In the case of the platinum compounds studied here it is of fundamental interest to examine how the two canonical modes of binding elucidated by crystallography are reflected in base-specific interactions. The presence of specific A-T interactions for non-covalent polynuclear platinum complexes is indicated by protection of the minor groove toward alkylation and is also confirmed (specifically for AH44) through 2D NMR experiments on the self-complementary duplex $d(GGTAATTACC)_2$, which is a 'high-affinity' sequence for minor-groove binders such as Hoechst 33258 and used extensively for solution and solid-state studies of 'classical' minor-groove binders (19).

Base-specific interactions were studied using predominantly TriplatinNC (AH78) given the similarities in behavior on random-sequence DNA observed above. There is a clear correlation between A·T content and the stabilizing effect of TriplatinNC (Figure 3). The difference in melting temperature increases with the amount of A·T base pairs from $\Delta T_M = +7.0°C$ for ctDNA to +22.6°C for *C. perfrin-*

Table 1. DNA binding properties of test compounds

Compound	C_{50} (μM)[a]	K_{app} (M^{-1})[b]	Q Hoechst[c]	Q Ethidium[c]	η/η_o[d]	ΔT_M (°C)[e]
Netropsin	44.26	2.50×10^6	03.31	22.55	1.007	+7.47 ± 0.50
Pentamidine	126.38	8.77×10^5	58.45	N/A	0.987	+0.03 ± 0.02
$[Co(NH_3)_6]Cl_3$	>300	N/A	23.18	273.62	0.828	+0.08 ± 1.12
AH78	1.96	5.65×10^7	N/A	4.88	0.385	+6.98 ± 0.02
AH78H	1.97	5.62×10^7	N/A	5.42	0.381	+8.20 ± 0.26
AH78P	2.14	5.18×10^7	N/A	5.07	0.443	+6.74 ± 0.64

[a] C_{50} = concentration required to reduce fluorescence by 50% during competitive ethidium bromide displacement assay on ctDNA.
[b] $K_{app} = K_b$ x 12.6/C_{50} where $K_b = 8.8 \times 10^6$ M(bp)$^{-1}$.
[c] Quenching of 50% initial fluorescence (μM) from limited DNA-bound dye.
[d] Relative viscosity at $r = 0.20$.
[e] ΔT_M = difference in thermal melting (T_m) (°C) of drug-treated CT-DNA at $r = 0.05$ compared with drug-untreated CT-DNA.

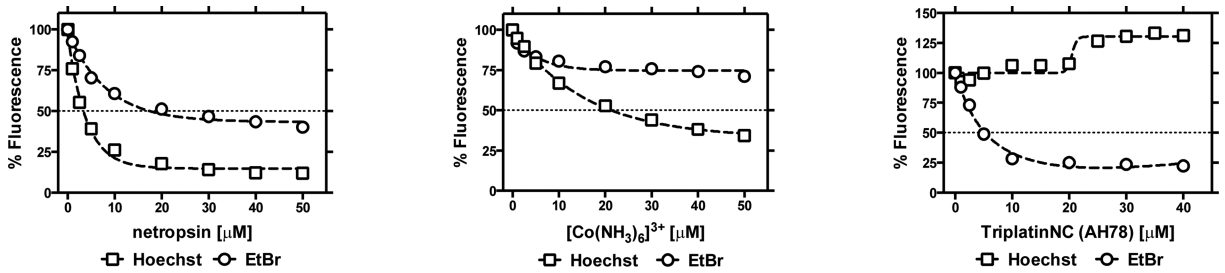

Figure 2. Normalized fluorescence quenching of limited ethidium bromide or Hoechst 33258 (5 μM) bound dsDNA (ctDNA) (25 μM) upon titration of minor-groove binding agents, netropsin and pentamidine, $[Co(NH_3)_6]Cl_3$ and the TriplatinNC (data points presented as an average of triplicate measurement, error bars ± SD).

	AT Content (%)	ΔT_m (°C)
CP-DNA	73	22.6
poly(dA)-poly(dT)	100	28.1
Poly[d(A-T)$_2$]	100	28.5

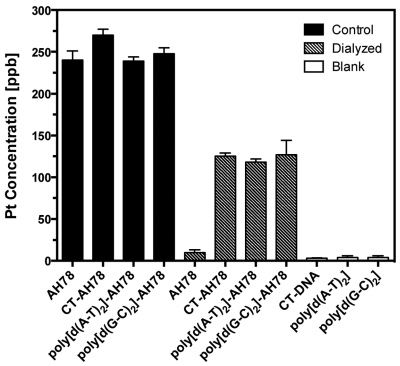

Figure 3. Thermal melting temperatures (at $r = 0.05$) of TriplatinNC on modified DNA (CP-DNA = *Clostridium perfringens* DNA) (left) and platinum concentration (in ppb) determined using ICP-MS on various DNA types (100 μM) upon treatment with TriplatinNC (5 μM) (right).

gens DNA (73% A·T), and then finally to > +28°C for pure A·T polynucleotides. To our knowledge such a high increase in melting temperature is unprecedented for a non-covalent DNA-binding small molecule at such low concentration ($r = 0.05$). It is noteworthy that the ΔT_M of TriplatinNC-modified homopolymeric and alternating copolymeric sequences are almost identical showing that stabilization arises from the discrete binding of TriplatinNC, and is not influenced by the initial melting temperature of the untreated polynucleotide. The associated binding strength of TriplatinNC to three sets of polymers—poly[d(G-C)$_2$], poly[d(A-T)$_2$] and poly(dA)-poly(dT)—was then identified through ICP-MS and revealed that platinum content is reduced by ∼50% after dialysis on all DNA types, but there is no apparent selectivity with base composition (Figure 3).

Fluorescence inhibition assay. A selection of double-stranded DNA polymers of varying G·C content—poly[d(G·C)$_2$] (100%), *Micrococcus lysodeikticus* DNA (ML-DNA; 72%), ctDNA (42%) and poly[d(A·T)$_2$] (0%)—was next examined under saturated EtBr competitive binding conditions (Supplementary Figure S4 and Table 2) to characterize potential base-specific binding constants. The classical agents netropsin and actinomycin D exhibited predictable behavior with the minor-groove binder favoring A·T-rich polymers while, conversely, the intercalator preferred G·C. Affinity values for netropsin and all trinuclear platinum compounds for the G-C and ML DNAs were similar to those found for ctDNA; see Tables 1 and 2. Unexpectedly, detectable binding constants (up to 500-μM exposure) were not obtained for poly[d(A·T)$_2$] for TriplatinNC. The congeners were then

examined and a detectable binding constant was observed only for AH78P ($K_{app} = 9 \times 10^5$ M(bp)$^{-1}$). This finding is in contrast to complex AH44 (Scheme 1) that displays some slight preference for A-T sequences when compared to nucleic acids of varying base composition (12). This evidence suggests that the DNA binding constants for the TriplatinNC class are dependent, and highly conserved, on polymers containing G·C content. But given the evidence of strong ΔT_m, questions now arise regarding the binding mode of this class toward conformationally distinct regions on DNA. Are there limited but high-affinity binding sites on A-T-rich tracts, and are the distinctive binding modes—groove spanning and backbone tracking—linked to base-specificity or tertiary helical topology, and if so, which of these modes are the drivers behind binding affinity and condensation? To probe these significant issues, further experiments on selected A·T and G·C polymers and oligonucleotides using circular dichroism, isothermal titration calorimetry (ITC) and 2D-NMR spectroscopy were undertaken.

Conformational changes. The changes in ellipticity of poly[d(A·T)$_2$] and poly[d(G·C)$_2$] with varying amounts of TriplatinNC are shown in Figure 4A and B and Supplementary Figure S6. The platinum compound significantly alters the secondary structure of poly[d(A-T)$_2$] with ellipticity of the band at 263.5 nm gradually diminishing upon complex treatment resulting in positive to negative shifts up to a drug loading ratio of 5% ($r = 0.05$). Furthermore, the appearance of a positive band around 290 nm at higher molar ratios—a wavelength where DNA normally does not absorb—indicates the formation of ψ-DNA. On the other hand, almost no change in the secondary structure of the poly[d(G·C)$_2$] polymer is induced upon TriplatinNC binding. The only significant alteration in the spectrum occurs at high drug loading when DNA condensation leads to ψ-DNA arrangement and subsequently precipitation takes place.

Negligible changes in the secondary structure of poly[d(G·C)$_2$] upon TriplatinNC binding were corroborated through competitive fluorescence binding analysis of mithramycin A; one of the few small molecules that binds to the minor groove of G-C-rich sequences (32,33). Binding of mithramycin A is not affected by the presence of TriplatinNC as fluorescence intensities of the DNA-bound antibiotic increase in a linear fashion to exactly the same extent for the TriplatinNC modified poly[d(G·C)$_2$], as for the untreated polynucleotide (Figure 4C). Control experiments confirmed that TriplatinNC did not interfere with the intrinsic fluorescence of mithramycin A itself (results not shown). This result confirms that TriplatinNC does not span the minor groove of poly[d(G·C)$_2$] and therefore does not prevent the interaction of other molecules within this region of DNA. Taken together these results suggest that although the association strength of TriplatinNC to A·T and G·C polynucleotides are indistinguishable, backbone tracking is the predominant binding mode for the G-C duplex. Minor-groove spanning interactions by the trinuclear platinum complexes, however, are characteristic of polynucleotides with A·T content. For example, cooperative enhancement of the minor-groove binding fluorophore Hoechst 33258 occurs for both ctDNA and, to a larger extent, poly[d(A·T)$_2$] (Figure 4D). ITC analysis lends further support toward the concept of selective groove spanning of A·T, rather than G·C, polynucleotides (Supplementary Figure S7). Not only do the shapes of the isotherms differ appreciably but also the generated reaction heat is about 10 times lower for the G·C polynucleotide (Supplementary Table S2). While a high signal-to-noise ratio of the poly[d(G·C)$_2$] isotherm made mathematical analysis unreasonable, analysis was possible for both poly[d(A·T)$_2$] and poly(dA)-poly(dT) isotherms (34,35). The curves of both A·T polynucleotides are very similar and show three reaction stages for binding, condensation and precipitation. Excluding the integrated heats of precipitation, isotherms were then fitted using a two-stage binding site model that revealed a highly exothermic condensation phase for both A·T polynucleotides (36).

NMR spectroscopy. Finally, 2D NMR spectroscopy was used to examine the binding modes using both an A-T-rich and a G-C-rich duplex (Supplementary Figure S8).

TriplatinNC-modified A-T duplex. The changes in the proton resonances for the A-T-rich dodecamer in the presence of TriplatinNC confirm that for both strands mainly the thymines and adenosines are affected by platinum drug binding (Supplementary Figures S9A and B). A preference of binding toward one strand over the other is not observed. The changes in chemical shifts for T-NH and T-CH3 result from structural changes of the dodecamer upon binding of TriplatinNC. In NOESY analysis there are many nuclear Overhauser effect (NOE) contacts between the TriplatinNC and the non-exchangeable protons of the oligonucleotide (Supplementary Figure S10). NOE cross peaks are observed with all A-H2 protons as connections seem to be stronger for TpNC-L2/L5 than L3/L4, suggesting that TriplatinNC spans/binds in minor groove, and there are strong connectivities with A-H1′ and T-H1′, and somewhat weaker contacts with C-H1′ (Figure 5). Cross-peaks with H2′/H2″ cannot be conclusively identified due to overlapping peaks but strong NOE contacts with H3′/H4′ and H5′/H5″ protons are present. These latter sugar connectivities in the proximity of the backbone phosphates point toward backbone binding. No cross-peaks with A-NH2 or C-NH2 or T-CH3 are visible indicating that major groove binding can be ruled out. Contacts to the imino protons of the nucleobases are also not detected. For the platinum compound, participation of the L1 protons is inconclusive since many H2″ protons have a similar chemical shift. Connectivities for NH_3/NH_2 groups of TriplatinNC with the oligomer are not observed. It is noteworthy that the NOE contacts between A-H2 protons and H2′/H2″ seem to be stronger in the presence of TriplatinNC. This could reflect the narrowing of the minor groove as a consequence of the binding of the platinum drug. In summary the results strongly suggest that TriplatinNC spans the minor groove.

Consequences for the TriplatinNC-modified GC duplex. In contrast to the AT duplex the changes in the GC-rich dodecamer upon binding of TriplatinNC are considerably smaller, with changes mainly occurring for the H1′ chemical

Table 2. Apparent DNA binding constants (K_{app}) of test compounds to dsDNA of varying A·T content

	K_{app} M(bp)$^{-1}$			
	poly[d(A·T)$_2$] (100% AT)	ctDNA (58% AT)	ML-DNA (28% AT)	poly[d(G·C)$_2$] (0% AT)
Actinomycin D	N/A	2.92×10^7	3.03×10^7	5.25×10^7
Netropsin	5.75×10^7	2.50×10^6	N/A	N/A
AH78	N/A	5.65×10^7	2.78×10^7	3.18×10^7
AH78H	N/A	5.62×10^7	1.44×10^7	1.95×10^7
AH78P	9.03×10^5	5.18×10^7	1.36×10^7	3.58×10^7

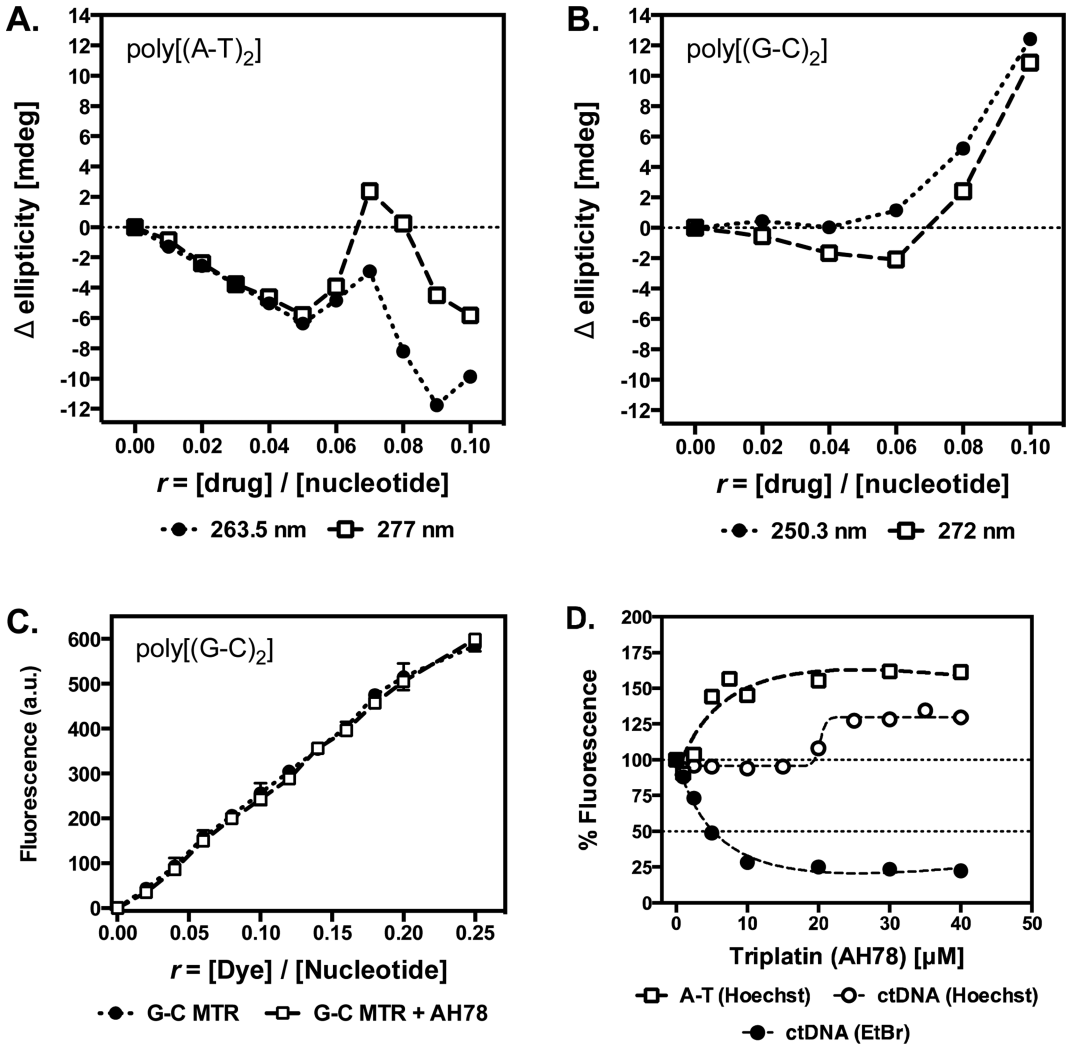

Figure 4. Changes in helical ellipticity of key absorbance bands upon treatment of poly[d(A-T)$_2$] (**A**) and poly[d(G-C)$_2$] (**B**) with TriplatinNC (AH78), the comparative binding of mithramycin A (MTR) to poly[d(G-C)$_2$] in the presence and absence of TriplatinNC (**C**) and quenching of limited bound Hoechst (5 μM) or ethidium bromide (5 μM) to ctDNA and poly[d(A-T)$_2$] (25 μM) polynucleotides (**D**).

shifts (Supplementary Figure S11). These shift variations arise most probably from induced structural changes since the spectra showed only a few contacts in the minor groove. Weak cross-peaks are observed between TpNC-L3/L4 and G-H8 and C-H6 as well as G-H1′ and C-H1′. The cross-peaks with H2′/H2″ sugar protons seem to be more pronounced but the strongest connectivities are observed in the H3′/H4′/H5′/H5″ region (Supplementary Figure S12). The fact that no connections with G-NH_2 or C-NH_2 are detected implies that binding via major or minor-groove spanning can be excluded. Connectivities between NH_2R/NH_3 protons of the platinum drug with the dodecamer cannot be detected. Overall these results suggest that TriplatinNC binds predominantly in a backbone-tracking manner toward GC-rich DNA.

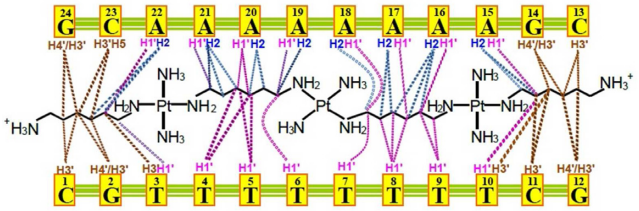

Figure 5. Summary of NOE contacts between TriplatinNC and the self-complementary A-T-rich duplex.

In summary, elucidation of solution binding by TriplatinNC and congeners to DNA clearly display two modes consistent with backbone tracking and groove-spanning interactions. What is clear from these experiments, and is of particular significance toward our understanding of novel 'non-covalent' platinum nucleic acid interactions, is that each mode is dependent on base specificity or local helical topological parameters. We suggest that backbone tracking is the predominant binding mode of TriplatinNC-type complexes in duplexes containing G-C nucleobases. Conversely, groove-spanning interactions are localized to the minor groove and are specifically dependent of A-T content. Furthermore, the groove-spanning motif has far greater impact on tertiary nucleic acid structure and is the main driver of DNA condensation and cooperative interactions at the minor groove.

Binding to yeast tRNA

To characterize Triplatin interactions with ribonucleic acid, and thus potentially differentiate binding activity with DNA, yeast tRNA was examined through fluorescence quenching experiments and thermal melting analysis. We initially characterized the intrinsic binding constant (K_b) of EtBr to tRNA using direct spectrophotometry at 260 nm as 6.78×10^4 M^{-1} (Supplementary Figure S1 and Supplementary Table S1) which is in good agreement with Sakai *et al.* (37). A fixed concentration of EtBr (12.6 μM) was then titrated against increasing concentrations of tRNA in order to identify the fluorescence saturation binding point (80.0 μM). Further, we then defined the apparent binding constant of tested samples to tRNA (K_{app}) within this method as; $K_{app} = K_b$ x $12.6/C_{50}$, where K_b is the intrinsic binding constant of EtBr to tRNA and C_{50} is the concentration (in μM) of tested agent required to displace 50% of the bound intercalated fluorophore (38,39). Quenching experiments were then examined with Triplatin complexes and $[Co(NH_3)_6]Cl_3$ titrated against EtBr-saturated tRNA solutions (Figure 6). Somewhat unexpectedly, only the pentanediamine Triplatin complex (AH78P) displaced 50% of bound EtBr and we estimate the binding constant of this agent to the fluorescent EtBr binding region of tRNA as 4.80×10^3 $M(bp)^{-1}$, an order of magnitude below the $[Co(NH_3)_6]Cl_3$ complex (7.95×10^4 $M(bp)^{-1}$). Indeed, electrostatic binding by $[Co(NH_3)_6]^{3+}$ to RNA has previously been identified on ribozyme (P4-P5-P6 portion) tandem G-U base pairs in the major groove (40). Thermal denaturation was then identified (Figure 6B and Supplementary Figure S13) with AH78P once again being the only platinum(II) complex to appreciably stabilize tRNA. Overall, the ability of Triplatin complexes to displace fluorogenically bound EtBr and stabilize thermal denaturation of tRNA appears favored by shorter linker chain length molecules. It is possible, however, that Triplatin molecules may bind tRNA at non-fluorescent EtBr binding sites (41) that have negligible influence on thermal denaturation. Atomic force microscopy (AFM) experiments on tRNA adducted by AH78 do indeed show condensation of the ribonucleotide but the results are not inconsistent if there is a subset of Triplatin binding sites different to those of EtBr (12).

Interactions with superhelical pUC19 and endonuclease inhibition

It is axiomatic that strong ligand binding to nucleic acids will interfere with protein recognition and processing. The effects of complex interactions on superhelical pUC19 plasmid DNA (pDNA) migration and subsequently sequence recognition by type II restriction endonucleases were examined. Agarose gel electrophoresis of superhelical pUC19 showed that the pentanediamine complex, AH78P, begins to inhibit plasmid migration at 0.50 μM with complete condensation occurring thereafter (Figure 7A). Higher concentrations of the longer hexanediamine AH78 and heptanediamine AH78H were required to initiate condensation (3.0 μM) while the metal-free ligand yielded no effect. The behavior by all Triplatin compounds here is entirely different to classical *cis*-platinum(II) and trinuclear BBR3464-type complexes. These agents covalently platinate superhelical pDNA and engage in concentration-dependent unwinding of the Form I superhelix (42–44).

To identify if Triplatin-bound DNA can prevent sequence recognition by type II restriction endonucleases, pUC19 was then linearized by the restriction enzyme AatII and subjected to a second endonuclease treatment of either BamHI, EcoRI or SalI, each of which also has one recognition sequence on pUC19 (Figure 7). The results of these control experiments are shown in Figure 7B where the linearized band of pUC19 at 2686 bp disappears and two smaller fragments emerge between 2188–2221 bp and 465–498 bp corresponding to site-selective excision. With Triplatin experiments, complexes were pre-incubated for 24 h at 37°C with linearized pUC19 at the range 1.0–10.0 μM for AH78 and AH78H, and between 0.25 and 1.00 μM for AH78P before the introduction of BamHI, EcoRI or SalI (Figure 7C–E). Triplatin complexes inhibit endonuclease excision in a concentration-dependent manner as characterized by the disappearance of pUC19 fragments at higher complex exposure. Inhibition is comparable between the hexanediamine- and heptanediamine-bridged AH78 and AH78H, respectively, where concentrations of 2.5 μM initiate condensation with bands becoming fainter and then disappearing >5 μM. The pentanediamine-linked AH78P displays a similar concentration-dependent inhibitory trend with the exception that lower concentrations (0.50 μM) are required to inhibition excision, before complete condensation occurs thereafter (0.75–1.00 μM). It is notable that Triplatin complexes do not preferentially inhibit cutting by any of these three site-specific endonucleases. Instead, the inhibitory properties are congruent, depending

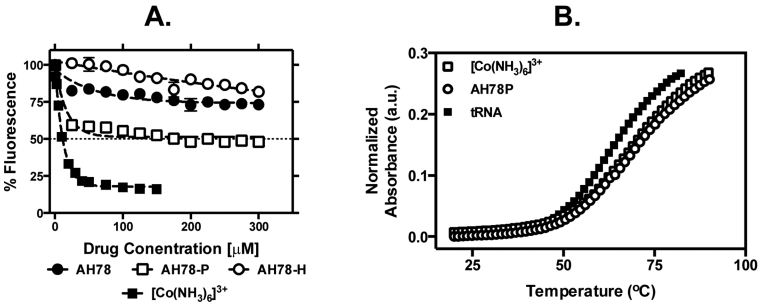

C.

Compound	C_{50} (μM) [a]	K_{app} (M^{-1})[b]	ΔT_m (°C)[c]
EtBr	-	-	+2.14 ± 0.31
$[Co(NH_3)_6]Cl_3$	10.74	7.95×10^4	+1.10 ± 0.10
AH78	>300		+0.20 ± 0.56
AH78H	>300		+0.13 ± 0.63
AH78P	177.61	4.80×10^3	+1.39 ± 0.60

Figure 6. (**A**) Competitive fluorescence binding of platinum complexes (AH78, AH78P and AH78H) and the cobalt(III) complex, $[Co(NH_3)_6]Cl_3$, to EtBr (12.6 μM) saturated solutions of transfer RNA (tRNA) (80 μM) (data points presented as an average of triplicate measurement, error bars ± SD). (**B**) Normalized thermal melting profiles of untreated tRNA (~130 μM in tRNAp) along with AH78P and $[Co(NH_3)_6]^{3+}$ treated (13 μM) tRNA examined in 50-mM potassium phosphate buffer with 1-M NaCl. (**C**) tRNA binding properties of test compounds. [a] C_{50} = concentration required to reduce fluorescence by 50% during competitive EtBr displacement assay [b] $K_{app} = K_b \times 12.6/C_{50}$ where $K_b = 6.78 \times 10^4$ $M(bp)^{-1}$ [c] ΔT_M = differential thermal melting (T_m) (°C) of drug-treated tRNA at $r = 0.10$ compared with drug-untreated tRNA.

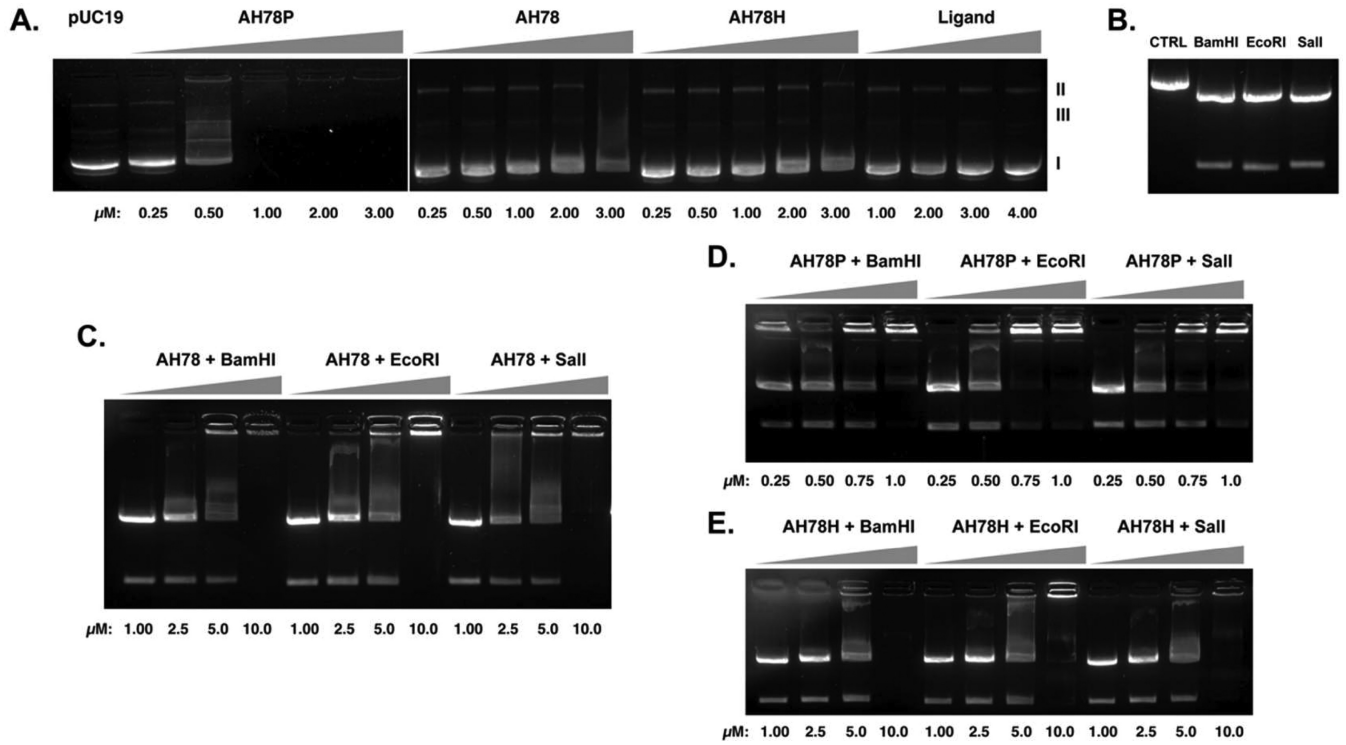

Figure 7. (**A**) Influence of Triplatin complexes and the metal-free ligand on superhelical pUC19 (400 ng) migration examined under agarose gel electrophoresis. (**B**) AatII linearized pUC19 (CTRL) after exposure to type II endonucleases. (**C–E**) Cleavage experiments on linearized pUC19, pre-incubated for 24 h with either; AH78 (1.0–10 μM), AH78P (0.25–1.0 μM) or AH78H (1.0–10 μM) by type II endonucleases BamHI, EcoRI and SalI.

only on complex concentration and the linker chain length (AH78P >> AH78 ≈ AH78H).

On-chip identification of endonuclease inhibition

Although the condensation effects of DNA by Triplatin complexes have clearly been demonstrated through changes in viscosity and gel electrophoresis in this study and also through AFM analysis in recent work (11,12), a question remains regarding the exact nature of endonuclease inhibition by the Triplatin series—condensation effects rendering both bands undetectable by gel electrophoresis should be distinguished from endonuclease inhibition through ligand (Triplatin)-DNA binding. In order to provide answers to this question, an on-chip DNA microfluidic method was devised using the Bioanalyzer 2100 platform (Agilent Technologies) and is shown in Supplementary Figure S14. The Bioanalyzer 2100 was selected due to its ability for high-resolution sizing and quantitation of dsDNA fragments through capillary electrophoresis (45,46) (http://www.agilent.com). We employed DNA 7500 microfluidic chips, designed to identify dsDNA fragments sized between 100 and 7500 bp, for the detection of endonuclease excision on linearized pU19 (2686 bp). Superhelical pUC19, initially linearized by the restriction enzyme AatII and purified using anion exchange chromatography, was then exposed to

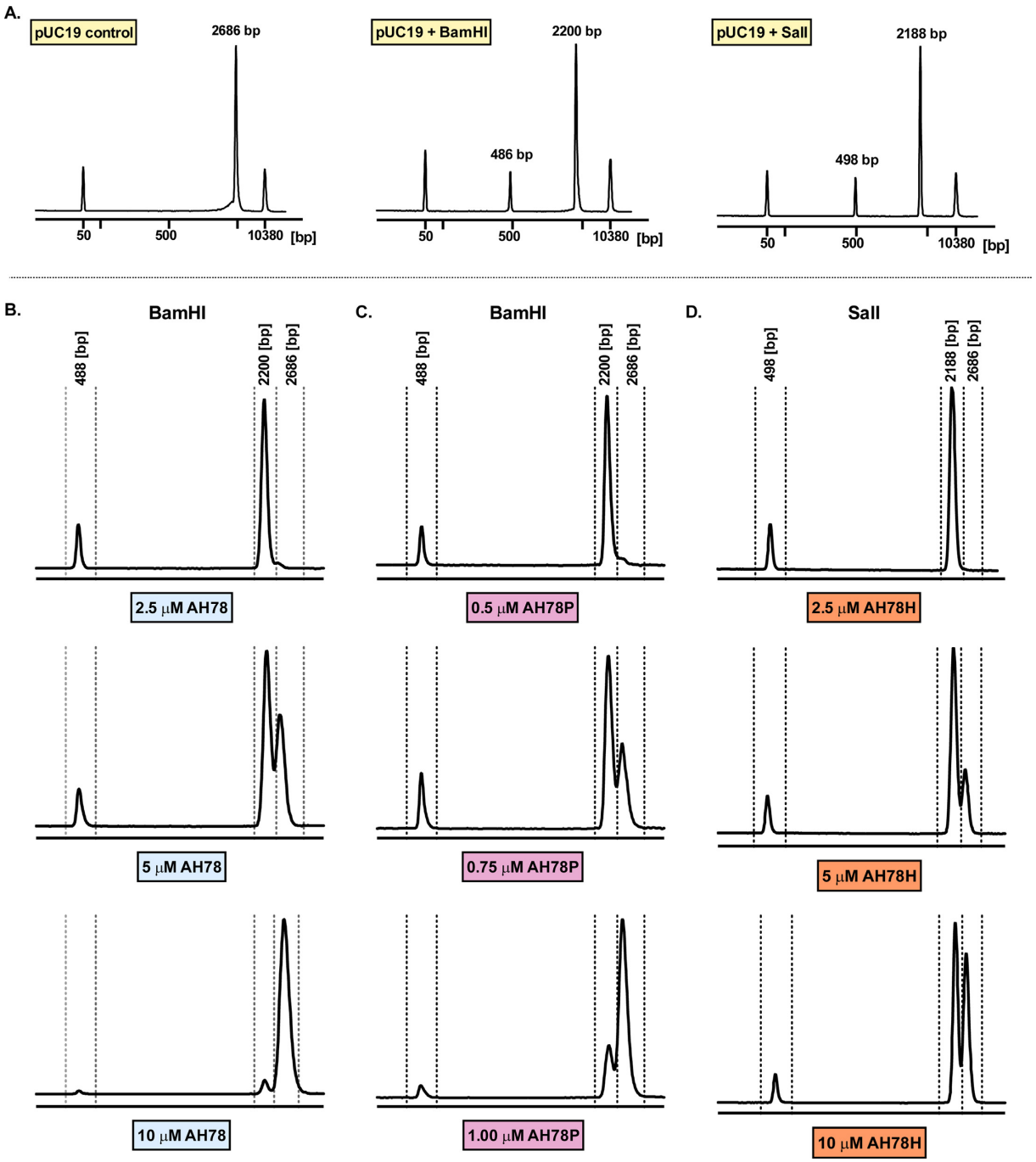

Figure 8. (**A**) Electrograms generated using the Bioanalyzer 2100 of AatII linearized pUC19 plasmid DNA with treatment by endonucleases BamHI and SalI. Electrograms of linearized pUC19 pre-incubated for 24 h with either AH78, AH78P or AH78H, followed by exposure over 2.5 h to the type II restriction endonuclease BamHI (**B**, **C**) or SalI (**D**).

two restriction endonucleases, BamHI and SaII, in a similar manner as described above.

Electrograms from the microfluidic chip analysis of untreated and enzyme-treated pUC19 are shown in Figure 8A and Supplementary S9. In each electrogram, internal standard upper and lower DNA markers sized at 50 and 10380 bp are evident. Linear pUC19 produced a single high-resolution peak located at ∼2870 bp which was clearly within the experimental error margin for nucleotide sizing accuracy (± 10% CV). Treatment by BamHI or SalI resulted in the disappearance of this band and the emergence of two smaller sequences located at ∼500 and ∼2200 bp which correspond to the expected site-selective enzymatic restriction activity. Triplatin complexes were then incubated for 24 h with linearized pUC19 (400 ng) prior to the exposure to BamHI or SalI. Tests were conducted in a similar manner to the electrophoresis experiments described above with AH78 and AH78H complexes being examined across

a higher range than AH78P (Figure 8B–D). Concentration-dependent endonuclease inhibition was identified in each set of experiments conducted. Taking complex AH78 with BamHI treatment as an example (Figure 8B): at lower complex concentrations of 1.0 and 2.5 μM the restriction enzyme efficiently cuts pUC19 into two smaller fragments and the results here are almost identical to the control experiment in Figure 8A. At higher concentrations however, the native pUC19 band at ∼2870 bp begins to appear and this band intensifies at the maximum exposure level (10 μM) as the BamHI excision fragments at ∼490 and ∼2200 bp diminish. Thus, in the presence of Triplatin complex, the pUC19 vector is protected from site-selective endonuclease excision. The trend observed in Figure 7C–E is largely present in these experiments, however, 10 μM of AH78H was unable to completely protect pUC19 from endonuclease excision by SalI (Figure 8D). On comparison with the agarose gel of this same experiment (Figure 7E), no bands are evident for pUC19 or the excision fragments. This indicates that complex AH78H has condensed both the native, or protected, plasmid along with the excised fragments. Another significant observation is the ability of AH78P to block endonuclease activity at nanomolar concentration levels (<1.0 μM) as evident in Figure 7C. The pentanediamine-bridged triplatinum(II) complex, therefore, has excellent selectivity for condensation and endonuclease inhibition on this dsDNA particular sequence (51% GC and 49% AT content).

CONCLUSIONS

The results here demonstrate the unique nucleic acid binding properties of 8+ charged 'non-covalent' PtN_4 type complexes binding through the phosphate clamp motif previously characterized by 'backbone tracking' and 'groove spanning' (1,2). The overall features from this and complementary studies (11,12) confirm that the crystallographically observed structures exist in solution and are relevant in explaining the biological activity of this series. The phosphate clamp, through its groove spanning, has apparent similarities to classical minor-groove binders (e.g. netropsin)—indicated by quenching of intercalated EtBr and stabilization of nucleic acid thermal denaturation, protection of the minor groove toward alkylation, (19), and the presence of many A-T minor-groove contacts observed through 2D NMR experiments on self-complementary A-T-rich duplexes (Figure 5; (19)). However, the phosphate clamp is distinguished by higher apparent binding constants to ctDNA and highly efficient condensation effects on both DNA and tRNA (11,12). The structural modifications of the phosphate clamp result in cooperative enhancement of minor-groove binders such as netropsin and Hoechst 32258. The base-specific studies allow differentiation between the dynamic effects of backbone tracking and groove spanning-backbone tracking is the predominant binding mode of TriplatinNC-type complexes in duplexes containing G-C nucleobases while, conversely, groove-spanning interactions are localized to the minor groove and are specifically dependent on A-T content. The latter has far greater impact on tertiary nucleic acid structure and the minor-groove residency of the platinum complex is the main driver of DNA condensation and cooperative interactions at the minor groove. The combined results further identify the phosphate clamp as a distinct mode of DNA binding, discrete from the canonical intercalator and minor-groove binders. The modular nature of the polynuclear chemotype allows for systematic modification of the chemotype. Apparent binding constants on ctDNA are identical among the series (K_{app} ∼5 x 10^7 M^{-1}) and are similar to recently reported non-terminally functionalized di- and tri-platinum(II): AH44 (Scheme 1), [{$Pt(NH_3)_3$}$_2$-μ-spermidine]$^{5+}$ and [{$Pt(NH_3)_3$}$_2$-μ-spermine]$^{6+}$ (K_{app} ∼3 x 10^7 M^{-1}). However, more subtle effects may be identified and in this study the slightly shorter pentanediamine-linked compound shows a number of effects (rapid interaction in competitive fluorescence experiments, EtBr displacement from tRNA, more efficient inhibition of pUC19 plasmid migration) suggesting the nucleic acid 'fit' may be modulated by the choice of diamine linker in this complex class. The combined effects of high binding constants and condensation effects of Triplatin complexes have significant consequences for inhibition of protein–DNA interactions. Type II restriction endonuclease inhibition on pUC19 was witnessed at G-G, G-A and G-T excision regions of BamHI, EcoRI and SalI enzymes in the presence of Triplatin-bound DNA. These results were visualized using agarose gel electrophoresis and then confirmed through the development of an on-chip microfluidic protocol for the Bioanalyzer 2100. There is again a distinct dependency on linker chain length with the pentanediamine complex inhibiting, or protecting, linearized pUC19 from digestion at the nanomolar exposure level while a 10-fold concentration increase (≥5.0 μM) by hexane- and heptane-bridged Triplatin cations was required to block restriction activity. In summary, the studies clearly display two modes of DNA binding consistent with backbone tracking and groove-spanning interactions where each mode is dependent on base specificity or local helical topological parameters.

SUPPLEMENTARY DATA

Supplementary Data are available at NAR Online.

FUNDING

Research Career Start Programme at Dublin City University, Irish Research Council [GOIPG/2013/937, GOIPG/2013/826]; EU COST Action: Biomimetic Radical Chemistry [CM1201]; National Institutes of Health (NIH) [RO1CA78754 to N.F.]. Funding for open access charge: NIH [RO1CA78754].
Conflict of interest statement. None declared.

REFERENCES

1. Komeda,S., Moulaei,T., Woods,K.K., Chikuma,M., Farrell,N.P. and Williams,L.D. (2006) A third mode of DNA binding: phosphate clamps by a polynuclear platinum complex. *J. Am. Chem. Soc.*, **128**, 16092–16103.
2. Komeda,S., Moulaei,T., Chikuma,M., Odani,A., Kipping,R., Farrell,N.P. and Williams,L.D. (2011) The phosphate clamp: a small and independent motif for nucleic acid backbone recognition. *Nucleic Acids Res.*, **39**, 325–336.

3. Takahara,P.M., Rosenzweig,A.C., Frederick,C.A. and Lippard,S.J. (1995) Crystal structure of double-stranded DNA containing the major adduct of the anticancer drug cisplatin. *Nature*, **377**, 649–652.
4. Klein,D.J., Schmeing,T.M., Moore,P.B. and Steitz,T.A. (2001) The kink-turn: a new RNA secondary structure motif. *EMBO J.*, **20**, 4214–4221.
5. Calnan,B.J., Tidor,B., Biancalana,S., Hudson,D. and Frankel,A.D. (1991) Arginine-mediated RNA recognition: the arginine fork. *Science*, **252**, 1167–1171.
6. Hurley,L.H. (2002) DNA and its associated processes as targets for cancer therapy. *Nat. Rev. Cancer*, **2**, 188–200.
7. Boer,D.R., Canals,A. and Coll,M. (2009) DNA-binding drugs caught in action: the latest 3D pictures of drug-DNA complexes. Dalton Trans. , 399–414.
8. Mangrum,J.B. and Farrell,N.P. (2010) Excursions in polynuclear platinum DNA binding. *Chem. Commun.*, **46**, 6640–6650.
9. Benedetti,B.T., Peterson,E.J., Kabolizadeh,P., Martínez,A., Kipping,R. and Farrell,N.P. (2011) Effects of noncovalent platinum drug-protein interactions on drug efficacy: use of fluorescent conjugates as probes for drug metabolism. *Mol. Pharm.*, **8**, 940–948.
10. Wedlock,L.E., Kilburn,M.R., Liu,R., Shaw,J.A., Berners-Price,S.J. and Farrell,N.P. (2013) NanoSIMS multi-element imaging reveals internalisation and nucleolar targeting for a highly-charged polynuclear platinum compound. *Chem. Commun.*, **49**, 6944–6946.
11. Malina,J., Farrell,N.P. and Brabec,V. (2014) DNA condensing effects and sequence selectivity of DNA binding of antitumor noncovalent polynuclear platinum complexes. *Inorg. Chem.*, **53**, 1662–1671.
12. Malina,J., Farrell,N.P. and Brabec,V. (2014) Noncovalent trinuclear platinum complexes efficiently condense/aggregate nucleic acids and inhibit enzymatic activity. *Angew. Chem.*, **53**, 12812–12816.
13. Harris,A.L., Yang,X., Hegmans,A., Povirk,L., Ryan,J.J., Kelland,L. and Farrell,N.P. (2005) Synthesis, characterization, and cytotoxicity of a novel highly charged trinuclear platinum compound. Enhancement of cellular uptake with charge. *Inorg. Chem.*, **44**, 9598–9600.
14. McCann,M., McGinley,J., Ni,K., O'Connor,M., Kavanagh,K., McKee,V., Colleran,J., Devereux,M., Gathergood,N., Barron,N. *et al.* (2013) A new phenanthroline-oxazine ligand: synthesis, coordination chemistry and atypical DNA binding interaction. *Chem. Commun.*, **49**, 2341–2343.
15. Prisecaru,A., McKee,V., Howe,O., Rochford,G., McCann,M., Colleran,J., Pour,M., Barron,N., Gathergood,N. and Kellett,A. (2013) Regulating bioactivity of Cu2+ bis-1,10-phenanthroline artificial metallonucleases with sterically functionalized pendant carboxylates. *J. Med. Chem.*, **56**, 8599–8615.
16. David Wilson,W., Tanious,F., Fernandez-Saiz,M. and Ted Rigl,C. (1997) Evaluation of drug-nucleic acid interactions by thermal melting curves. In: Fox,KR (ed). *Methods in Molecular Biology™*, Springer, NY, **90**, pp. 219–240.
17. Barceló,F., Ortiz-Lombardía,M. and Portugal,J. (2001) Heterogeneous DNA binding modes of berenil. *Biochim. Biophys. Acta*, **1519**, 175–184.
18. Remeta,D.P., Mudd,C.P., Berger,R.L. and Breslauer,K.J. (1993) Thermodynamic characterization of daunomycin-DNA interactions: comparison of complete binding profiles for a series of DNA host duplexes. *Biochemistry*, **32**, 5064–5073.
19. Qu,Y., Moniodis,J.J., Harris,A.L., Yang,X., Hegmans,A., Povirk,L.F., Berners-Price,S.J. and Farrell,N.P. (2012) Non-covalent polynuclear platinum compounds as polyamine analogs. In: Woster,P and Casero,R (eds). *Polyamine Drug Discovery*, RSC Drug Discovery Series No. 17, pp. 191–204.
20. Qu,Y., Scarsdale,N.J., Tran,M.-C. and Farrell,N. (2003) Cooperative effects in long-range 1,4 DNA-DNA interstrand cross-links formed by polynuclear platinum complexes. An unexpected *syn*-orientation of adenine bases outside the binding sites. *J. Biol. Inorg. Chem.*, **8**, 19–28.
21. Carter,M.T., Rodriguez,M. and Bard,A.J. (1989) Voltammetric studies of the interaction of metal chelates with DNA. 2. Tris-chelated complexes of cobalt (III) and iron (II) with 1, 10-phenanthroline and 2, 2'-bipyridine. *J. Am. Chem. Soc.*, **111**, 8901–8911.
22. Marty,R., N'soukpoé-Kossi,C.N., Charbonneau,D.M., Kreplak,L. and Tajmir-Riahi,H.-A. (2009) Structural characterization of cationic lipid-tRNA complexes. *Nucleic Acids Res.*, **37**, 5197–5207.
23. Wang,A.H.-J. (1992) Intercalative drug binding to DNA. *Curr. Opin. Struct. Biol.*, **2**, 361–368.
24. Bailly,C., Colson,P., Hénichart,J.-P. and Houssier,C. (1993) The different binding modes of Hoechst 33258 to DNA studied by electirc linear dichroism. *Nucleic Acids Res.*, **21**, 3705–3709.
25. Luck,G., Triebel,H., Waring,M. and Zimmer,C. (1974) Conformation dependent binding of netropsin and distamycin to DNA and DNA model polymers. *Nucleic Acids Res.*, **1**, 503–530.
26. Luedtke,N.W., Hwang,J.S., Nava,E., Gut,D., Kol,M. and Tor,Y. (2003) The DNA and RNA specificity of eilatin Ru(II) complexes as compared to eilatin and ethidium bromide. *Nucleic Acids Res.*, **31**, 5732–5740.
27. Kankia,B.I., Buckin,V. and Bloomfield,V.A. (2001) Hexamminecobalt(III)-induced condensation of calf thymus DNA: circular dichroism and hydration measurements. *Nucleic Acids Res.*, **29**, 2795–2801.
28. Lerman,L.S., (1961) Structural considerations in the interaction of DNA and acridines. *J. Mol. Biol.*, **3**, 18–30.
29. Cohen,G. and Eisenberg,H., (1969) Viscosity and sedimentation study of sonicated DNA–proflavine complexes. *Biopolymers*, **8**, 45–55.
30. Cheatham,T.E. and Kollman,P.A. (1997) Insight into the stabilization of A-DNA by specific ion association: spontaneous B-DNA to A-DNA transitions observed in molecular dynamics simulations of $d[ACCCGCGGGT]_2$ in the presence of hexaamminecobalt(III). *Structure*, **5**, 1297–1311.
31. Harris,A., Qu,Y. and Farrell,N.P. (2005) Unique cooperative binding interaction observed between a minor groove binding Pt anti-tumor agent and Hoeschst Dye 33258. *Inorg. Chem.*, **44**, 1196–1198.
32. Sastry,M., Fiala,R. and Patel,D.J. (1995) Solution structure of mithramycin dimers bound to partially overlapping sites on DNA. *J. Mol. Biol.*, **251**, 674–689.
33. Geierstanger,B.H. and Wemmer,D.E. (1995) Complexes of the minor groove of DNA. *Annu. Rev. Biophys. Biomol. Struct.*, **24**, 463–493.
34. Matulis,D., Rouzina,I. and Bloomfield,V.A. (2000) Thermodynamics of DNA binding and condensation: isothermal titration calorimetry and electrostatic mechanism. *J. Mol. Biol.*, **296**, 1053–1063.
35. Kim,W., Yamasaki,Y. and Kataoka,K. (2006) Development of a fitting model suitable for the isothermal titration calorimetric curve of DNA with cationic ligands. *J. Phys. Chem. B*, **110**, 10919–10925.
36. Wilson,R.W. and Bloomfield,V.A. (1979) Counter ion-induced condensation of deoxyribonucleic acid: a light-scattering study. *Biochemistry*, **18**, 2192–2196.
37. Sakai,T.T., Torget,R., Josephine,I., Freda,C.E. and Cohen,S.S. (1975) The binding of polyamines and of ethidium bromide to tRNA. *Nucleic Acids Res.*, **2**, 1005–1022.
38. Jones,C.R., Bolton,P.H. and Kearns,D.R. (1978) Ethidium bromide binding to transfer RNA: transfer RNA as a model system for studying drug-RNA interactions. *Biochemistry*, **17**, 601–607.
39. Olmsted,J. and Kearns,D.R. (1977) Mechanism of ethidium bromide fluorescence enhancement on binding to nucleic acids. *Biochemistry*, **16**, 3647–3654.
40. Kieft,J.S. and Tinoco,I. (1997) Solution structure of a metal-binding site in the major groove of RNA complexed with cobalt (III) hexammine. *Structure*, **5**, 713–721.
41. Liebman,M., Rubin,J. and Sundaralingam,M. (1977) Nonintercalative binding of ethidium bromide to nucleic acids: crystal structure of an ethidium-tRNA molecular complex. *Proc. Natl Acad. Sci. U.S.A.*, **74**, 4821–4825.
42. Bellon,S.F., Coleman,J.H. and Lippard,S.J. (1991) DNA unwinding produced by site-specific intrastrand crosslinks of the antitumor drug cis-diamminedichloroplatinum(II). *Biochemistry*, **30**, 8026–8035.
43. Brabec,V., Kaspárková,J., Vrána,O., Nováková,O., Cox,J.W., Qu,Y. and Farrell,N. (1999) DNA modifications by a novel bifunctional trinuclear platinum phase I anticancer agent. *Biochemistry*, **38**, 6781–6790.
44. Ruhayel,R.A., Langner,J.S., Oke,M.-J., Berners-Price,S.J. and Zgani,I. (2012) Chimeric platinum-polyamines and DNA binding. Kinetics of DNA interstrand cross-link formation by dinuclear platinum complexes with polyamine linkers. *J. Am. Chem. Soc.*, **134**, 7135–7146.
45. Molphy,Z., Prisecaru,A., Slator,C., Barron,N., McCann,M., Colleran,J., Chandran,D., Gathergood,N. and Kellett,A. (2014) Copper phenanthrene oxidative chemical nucleases. *Inorg. Chem.*, **53**, 5392–5404.
46. Wang,J. (2000) From DNA biosensors to gene chips. *Nucleic Acids Res.*, **28**, 3011–3016.